

Durability prediction of an ultra-large mining truck tire using an enhanced finite element method

Nyaaba, W., Bolarinwa, E. & Frimpong, S. Author post-print (accepted) deposited by Coventry University's Repository

Original citation & hyperlink:

Nyaaba, W, Bolarinwa, E & Frimpong, S 2018, 'Durability prediction of an ultra-large mining truck tire using an enhanced finite element method' Proceedings of the Institution of Mechanical Engineers, Part D: Journal of Automobile Engineering, vol. (In-Press), pp. (In-Press).

https://dx.doi.org/10.1177/0954407018795278

DOI 10.1177/0954407018795278 ISSN 0954-4070 ESSN 2041-2991 Publisher: Sage

Copyright © and Moral Rights are retained by the author(s) and/ or other copyright owners. A copy can be downloaded for personal non-commercial research or study, without prior permission or charge. This item cannot be reproduced or quoted extensively from without first obtaining permission in writing from the copyright holder(s). The content must not be changed in any way or sold commercially in any format or medium without the formal permission of the copyright holders.

This document is the author's post-print version, incorporating any revisions agreed during the peer-review process. Some differences between the published version and this version may remain and you are advised to consult the published version if you wish to cite from it.

Durability Prediction of an Ultra-Large Mining Truck Tire using an Enhanced Finite Element Method

Abstract

Ultra-class mining trucks used for material haulage in rugged surface mining terrains experience premature tire fatigue failures. Typical failures include belt edge separation, ply turn-up separation, tread base, and sidewall cracking. The use of reinforcing fillers and processing aids in tire compounds result in the formation of microstructural in-homogeneities in the compounds. This paper presents an application of the critical plane analysis technique for predicting the fatigue life of the belt package of an ultra-large mining truck (CAT 795F) tire of size 56/80R63 in a surface coal mine. Experimental data obtained from extracted specimens (sidewall, tread, and belt-edge region) of an in-service tire is used to characterize the stress-strain and fatigue behavior of the modeled tire. The tire's duty cycle stresses and strains were obtained from finite element analysis of the rolling tire in ABAQUS. Fatigue life calculations were performed in the rubber fatigue solver Endurica CL. Effects of inflation pressure, tire speed, and axle load on the fatigue life of the belt package under strain crystallizing and non-crystallizing conditions of the belt compound are discussed. Specifically, the results show the belt edges to be critical regarding crack nucleation. **Keywords:** Mining Truck Tire, Rubber, Finite Element Method, Critical Plane Analysis, Fatigue Life, Strain-induced Crystallization, Belt Package

1. Introduction

The benefits in cost savings associated with the use of heavy mining machinery in the surface mining industry have resulted in the production of ultra-large radial tires with rim diameters above 0.89 m. The harsh environmental and loading conditions mining tires are exposed to could be the reason for their frequent maintenance and subsequent premature failures. Common fatigue failure forms in these tires are sidewall cracking, caused by ozone attack; tread groove cracking, belt edge separation, and bead rubber erosion (wear).

Several fundamental and applied research initiatives have been carried out in the area of tire durability studies in recent years. Particularly, a continuum damage -based approach has been used to assess tire durability limits at varying degrees of complexities. Continuum damage approach factors material point stress and strain quantities into determining crack initiation life. For a known crack of relatively large size, an explicit crack feature can be introduced in a finite element model to obtain the propagation life based on the crack tip strain energy release rate using the theory of fracture mechanics.¹⁻⁴Although approximate, Näser et al.⁵ have shown that tire durability predictions cannot solely be dependent on

2

fracture mechanics parameters but also on other factors, such as strain-induced crystallization (SIC).

It is assumed in this work that crack originator sizes are geometrically small relative to the global tire dimensions,^{6, 7} hence the effects of loads on a crack precursor at the finite elements centroids may be analyzed without explicitly including the crack as a unique feature in the finite element mesh.⁸ The virtual crack precursors assume the planes and orientations of the applied loads. Mars⁸ reported that not all the elastically stored energy at a point on a given cracking plane is available to be released during cracking, especially when the strain state is multiaxial. Thus, the cracking energy density parameter, a fraction of the total strain energy density, is used to account for the effects of multiaxial loading experienced by each possible cracking plane in this work. A key to this fatigue life investigation effort is the application of the critical plane analysis technique to determine which initiation plane at each material point will be most damaged based on the loading history. The present work uses the continuum damage mechanics to accurately predict the fatigue life of the reinforced components of the 56/80R63 size tire for the CAT 795F haul truck ⁹ in a surface coal mine. The effects of strain crystallization on fatigue life prediction are also included in the study. The study is a pioneering effort which contributes to the body of knowledge in mining dump truck tire durability.

The first part of the paper focuses on material tests and calibration of experimental data for the finite element (FE) model. Details of the FE model geometry and mesh are discussed next. This is followed by a discussion on the critical plane technique in predicting fatigue life. The paper ends with sections on results discussion and conclusions.

2. Material Characterization

Specimens were extracted from different regions of an in-service tire namely belt, sidewall, tread, inner-liner, and apex for testing. The mechanical properties investigated during testing included stress-strain, stress relaxation, and fatigue crack growth. Due to specimen size limitations, only the belt compound was tested for fatigue crack growth. Note that the belt compound was assumed for the casing as well.

2.1 Stress-Strain Behavior

A simple tension (ST) measurement was carried out on each skived out compound (specimen size: 100 mm x 10 mm x 2 mm). Each specimen was tested at five strain levels (10%, 20%, 40%, 60%, and 100%) using an Elastomer Tension W400 testing apparatus. The testing consisted in stretching a specimen at 0.01/s strain rate up to a targeted strain level, followed by unloading at the same strain rate to a near-zero stress condition. The direction of

stretching was chosen along the longest dimension to ensure a state of pure strain in the specimen. In order to fully characterize the stress-strain behavior of the compounds, the theory of isotropic linear elasticity was used to establish relationships that allowed planar tension (PT) and equibiaxial tension (ET) data to be derived from the ST stress data. Essentially, a factor of 1.3 and 2 was applied to the ST data to obtain the PT and ET data, respectively.¹⁰

For each compound, the three sets of stress-strain data were fitted to the Ogden¹¹ hyperelastic law given in Eq. (1). The strain energy density W, in Eq. (1), is defined in terms of the deviatoric principal stretches $\overline{\lambda}_i$, the number of terms in the model N, and the model parameters μ_i , and α_i . In Fig. 1, the curves of the three deformation modes of the belt compound are shown to represent the multiaxial strain state captured in the finite element model. The belt compound is only used as a representation of similar behaviors observed in the other compounds.

$$W = \sum_{i=1}^{N} \frac{2\mu_i}{\sigma_i^2} \left(\overline{\lambda}_1^{\alpha_i} + \overline{\lambda}_2^{\alpha_i} + \overline{\lambda}_3^{\alpha_i} - 3 \right)$$
(1)

[Insert Fig. 1— Belt compound stress-strain plot]



Specimens were stretched in simple tension at a set a 20% strain level while stress data was collected over a period of 2,000 s. It was assumed that the relaxation rate, in each compound, was proportional to the applied strain, hence the choice of the Prony series model for training the resulting stress-time data. Modeling the viscoelastic behavior of the compounds was only

Regions	Ogden Model Constants						Prony Series Constants			
	μ ₁	α1	μ ₂	α2	μ ₃	α3	g_1	g_2	τ ₁	τ2
Apex	1.59E-3	-7.761	0.020	12.448	2.277	-0.2016	0.09	0.13	2.33	101.67
Belt	1.148	0.039	0.005	11.249	0.007	-4.734	0.092	0.104	7.089	253.51
Innerliner	2.83E-4	-7.966	0.015	9.837	0.424	-0.352	0.128	0.129	8.62	235.55
Sidewall	2.66E-4	-7.362	0.004	11.364	1.031	-0.099	0.105	0.125	8.037	289.04
Tread	0.0015	-5.332	0.012	8.920	1.229	-0.107	0.057	0.067	8.007	322.93

Table 1. Tire compounds hyperelastic and Prony series constants.

essential for the dynamic rolling simulation conducted on the tire. Table 1 summarizes both the hyperelastic and Prony series constants obtained for each tire compound. It should be noted that the material constants in Table 1 were obtained from curve-fitting the Ogden and Prony series models to the measurement data. The tire finite element model, discussed later on, was built on the material data in Table 1.

2.3 Fatigue Crack Growth (FCG)

Considering that filled natural rubber (NR) used in the belt region of the tire strain crystallizes upon application of non-relaxing loads,⁵ FCG measurements were taken under fully relaxing and non-relaxing conditions in a static tearing energy experiment. A planar tension specimen with a pre-cut length of 25 mm was cycled through varying strain levels and the crack length measured at the end of each cycle. Fig. 2 shows the maximum strain, maximum stress and crack growth length data collected during the fully relaxing experiment. In the absence of information on the fatigue threshold,¹² requiring a separate and specialized testing technique, the Thomas¹³ crack growth rate law (Eq. 2) was used for the fatigue life calculations. The fatigue crack growth rate (FCGR), $\frac{dc}{dN}$, was obtained from fitting a power-law to the crack growth data in Fig. 2c. The FCGR of the compound is dependent on the energy release rate *T*. *F* is the slope of the power-law curve. Note that T_c and r_c are material constants representing, respectively, the fracture strength of the compound and maximum fatigue crack growth rate corresponding to T_c .¹⁴

$$\frac{dc}{dN} = r_c \left(\frac{T}{T_c}\right)^F \tag{2}$$

[Fig. 2a — Maximum applied strain.]
[Fig. 2b — Maximum applied stress.]
[Fig. 2c — Crack growth length.]

Subsequently, fatigue crack growth rate data was generated based on Eq. (2) and plotted on a double logarithmic scale as a function of peak tearing energy. Fig. 3 shows the FCGR for both the loading and unloading strokes of the experiment.

2.3.1 Strain Crystallization

To assess the benefits of strain-induced crystallization (SIC) at the crack tip,^{14, 15} FCG test on the specimen was repeated under conditions that minimum strains were non-zero parts of the experiment. The test begins with growing a crack under fully relaxing conditions and then arresting the growth by ramping up the cycle minimum strains. Crack growth tends to retard in strain crystallizing materials under situations where $\frac{T_{\text{min}}}{T_{\text{max}}} = R > 0.5$

[Fig. 3 — Fatigue crack growth rate plot – fully relaxing loading.]

In Fig. 4a, a representative plot of maximum and minimum strains measured at a predefined number of cycles is shown for one of the crack growth rates considered in the test. As shown in Fig. 4b, the crack grows steadily at the beginning when fully relaxed loads are applied until after 40,000 cycles when the ramped up minimum strains cause the growing crack to retard. In modeling the effects of SIC in the belt compound, the pioneering work of Mars and Fatemi¹⁴ was followed. Here, the dependence of the fatigue crack growth rate on R-ratio is introduced in the power-law slope F of Eq. (2) as follows.

$$\frac{dc}{dN} = r_c \left(\frac{T}{T_c}\right)^{F(R)}$$
(3)

Next, Eq. (3) is rearranged to yield Eq. (4) for plotting F as a function of R-ratio, as shown in Fig. 5. A cubic polynomial function was then fitted to the experimental data such that F(R) could be represented in the form given in Eq. (5). Note that F_o is the fully relaxing power-law slope, which is approximately 2 for most NR compounds.

$$F(R) = \frac{\log\left(\frac{dc/dN}{r_c}\right)}{\log\left(\frac{T_{\max}}{T_c}\right)}$$
(4)

[Fig. 4a — Maximum and minimum applied strains.] [Fig. 4b — Crack growth and retardation.]

$$F(R) = F_0 + F_1 R + F_2 R^2 + F_3 R^3$$
(5)

Fig. 6 shows plots of fatigue crack growth rate curves for different *R*-ratios. It is evident in the plots that for R > 0, the rate of crack growth decreases for any given energy release rate in the strain crystallizing material.

[Insert Fig. 5 — Effect of R ratio on power-law slope *F*.] [Insert Fig. 6 — Effect of SIC on fatigue crack growth rate.]

3. Finite Element Model of the 56/80R63 Tire

A treaded 3D finite element (FE) model of the 56/80R63 tire was developed from an axisymmetric model during the inflation loading step of the analysis. Both models are shown in Fig. 7. The axisymmetric model consisted of 14,771 nodes and 9,062 elements of the type

CGAX4R/CGAX3R with a twist degree of freedom. Allowing twist in the model was necessitated by the anisotropy associated with the fiber reinforcements¹⁶. The inner casing was modeled as a single steel-corded ply having a bias angle of 0°. The belt package comprising six belt layers was modeled to assume a pyramidal shape, the widest layer being the transition belt layer (radially innermost belt).¹⁷ The bead region is often modeled with small elements of high stiffness which results in extremely small stable time increments in the explicit time integration scheme used in the rolling simulation. In the current model, the high stiffness rim and bead structures were modeled as rigid bodies connected to the axle through a reference node. Total nodes and elements used in the 3D model were 1,247,083 and 1,051,007, respectively, consisting of reduced integration linear brick elements (C3D8R), and quadrilateral surface (SFM3D4R) and membrane (M3D4R). Details on the model validation and verification are provided in reference.¹⁰ Strains to be used in the fatigue calculation step were required to be recovered in a given local coordinate system consistent with those specified for elements in the finite element model.

The rolling analysis conducted considered prevailing operating conditions at a US coal mine. The compact and even haul road surfaces meant an analytically rigid surface suffices to be used as a haul road in the simulation experiments. The straight-line rolling analysis set up included specifying a vertical load and velocity boundary condition at the rim

center reference node. A traction torque was applied around the wheel axle at an angular velocity ω defined by the dynamic loaded radius of the tire and the truck travel velocity. A front right wheel position tire of the CAT 795F rigid body dump truck was investigated under varying internal pressure and speed conditions. Notably, three inflation loads: 724 kPa, 793 kPa and 827 kPa were considered under a constant axle load of 1.01 MN except for the case where the truck travels unloaded at a vertical load of 0.6 MN.

[Fig. 7a — Finite element model of a 56/80R63 tire – axisymmetric model in Abaqus. [Fig. 7b — Finite element model of 56/80R63 tire – full model in Abaqus.]

For each inflation pressure and axel load combination, the tire was rolled under three different speed cases: (1) on-grade loaded travel speed -3.6 m/s, (2) on-a-flat stretch of road loaded travel speed -12.07 m/s, and (3) on-a-flat stretch of road empty travel speed -14.4 m/s. The carefully selected speed conditions represent the average speeds allowed on the mine property for the ultra-large haulage trucks. In all cases, a friction coefficient of 0.7 was assumed to exist between the tread and road surface. The nominal strain histories obtained from the FE rolling analysis were later used for the fatigue prediction. The FE model set up and analyses were conducted in Abaqus.

4. Critical Plane Analysis Method

As evident in most fatigue crack growth tests under small crack and uniaxial loading conditions, the energy release rate is approximated by the product of the strain energy density and crack size. Fatigue life is then calculated by integrating the crack growth rate of the weakest material point from its initial size to its critical size. In essence, this fatigue life prediction approach considers the total strain energy density at a material plane to be the driving force for crack growth. Mars⁸, however, showed that for a multiaxial strain state situation, not all the strain energy density is available to be released on the cracking plane and therefore proposed a cracking energy density (CED) function for multiaxial loading situations. For a given failure plane in the model, Fig. 8 shows a comparison of the available strain and cracking energy densities. Detailed derivation of the CED function is provided in Mars⁸ but only mentioned in the present work to show its implementation.

[Fig. 8 — Strain and cracking energy densities of a given failure plane.]

Incrementally, CED is defined as given in Eq. (6), where σ and $d\varepsilon$ are the traction vector and strain increment vector, respectively on a given material plane. \vec{r} is the unit normal vector to the material plane.

13

$$dW_c = \vec{r}^T \sigma d\varepsilon \vec{r} \tag{6}$$

It is worth noting that CED is independent of the strain path and thus, allows computation of crack tip loading histories along arbitrary material plane orientations. Consequently, the available energy release rate to grow a crack precursor occurring on a material plane of arbitrary orientation can be obtained from Eq. (7).

$$T = 2\pi W_c c \tag{7}$$

 W_c and c are the history of the CED and size of the crack, respectively, on a given cracking plane of some orientation. With the local crack driving force T, the fatigue life of a material plane can be obtained by integrating the growth rate in Eq. (2) from a known initial flaw size c_o to a critical size c_f according to Eq. (8). It has been established in practice that when $c_o \ll c_f$, the estimated life is insensitive to the critical flaw size c_f .⁸

$$N = \int_{c_o}^{c_f} \frac{1}{f(T(c, W_c))} dc \tag{8}$$

When a rubber specimen is subjected to multiaxial loads, the CED experienced by each virtual crack precursor is mainly dependent on the cracking plane orientation defined by its unit normal vector. Thus, a procedure that takes into account the strain history, hyperelastic constitutive model, and the energy release rate of a given material plane is vital in predicting the fatigue life of a crack precursor of a known size occurring on that plane at varying orientations. The plane whose orientation gives the shortest fatigue life is considered the critical plane. This procedure constitutes the critical plane analysis method. In this work, the critical plane search algorithm implemented in the rubber fatigue solver, Endurica CL was used to predict the fatigue life of critical regions in the belt package of the tire being studied. In Fig. 9a, it is shown that the domain of search is the unit half sphere and its coordinates θ and ϕ determine the potential failure plane orientation \vec{r} . Here, fatigue life is seen to depend on plane orientation. Note that life (in repeats of tire revolution) on the unit damage sphere corresponds to $\log_{10}(N)$ and each point on the sphere is a unit normal vector of a potential failure plane. When ϕ is set to a constant, fatigue life varies with the different instances of θ as shown in Fig. 9b.

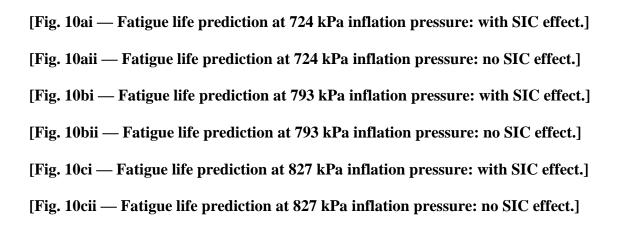
[Fig. 9a — Fatigue life dependence on failure plane orientation: domain of search.]

[Fig. 9b — Fatigue life dependence on damage sphere coordinate θ .]

5. Tire Performance and Fatigue Life Analysis

The initial crack size c_o was determined to be 0.08 mm according to the mine average tire replacement life of 8,500 hrs (8.5×10^6 revolutions) at 3.6 m/s travel speed. Even though the resultant strains obtained from the rolling analysis were not axisymmetric, it was imperative that a representative cross-section of the full model be used for the fatigue life calculations to save time, as well as enhance results visualization. Thus, a script was written to import strains from the 3D solid elements into their corresponding axisymmetric elements for the fatigue life predictions.

For the belt package analyzed, rolling simulation was defined in terms of the empty travel speed of 14.4 m/s but at different inflation loads. The results of the fatigue life predictions are shown in Fig. 10, where each sub-figure has life estimates of the belt compound with or without the inclusion of the effects of strain crystallization. In all the three loading cases, the belt edges were shown to be the most critical regions for crack initiation and subsequent propagation. This observation is consistent with results in the literature¹⁸ identifying the belt edges to be zones of high damage accumulation as a result of the weak bonding between the cords and the surrounding rubber.



Notably, fatigue life improved significantly when the effects of strain crystallization were included in the model across the different inflation pressures. At 724 kPa internal pressure, the strain-crystallizing compound's life reduced from 6.298×10^7 to 3.635×10^7 , which represents a 42% reduction in life in the absence of SIC (Fig. 10a). The same trend was observed for the other two inflation loads, where a magnitude of life reduction was recorded at 793 kPa and 827 kPa pressures, as shown respectively in Fig. 10b and Fig. 10c. In general, critical regions varied from one location to another in the vicinity of the belt edges, an observation which can be attributed to the effects of inertia. Again, a closer look at the contour plots of the strain-crystallizing (with output variable: Life_W/_SIC) model results, at 724 kPa pressure, crack is seen to initiate on top of the transition (innermost) belt at a location 145 mm away from the belt end. Similarly, delamination is observed to be likely at

the interface of the second and third working belts (Fig. 10c). Consistent with Näser et al.⁵ proposition, the life predictions when SIC effects are considered tend to improve significantly with increasing inflation loads. They attributed the non-relaxing loads (R > 0) at a crack tip when it passes through the footprint to the internal pressure of the tire. Thus, fatigue life is improved in strain-crystallizing compounds used in tires at relatively high inflation pressures. Regardless of the improvement in fatigue life, over inflating mining tires may cause them to damage more easily, especially when they run over road debris.

In determining the optimum inflation pressure for the operation, CED plots of the tire's duty cycle were obtained for the three inflation cases under loaded and unloaded truck conditions at a constant translational velocity of 14.4 m/s. In Fig. 11a, at full rated vertical axle load, the peak crack driving force (CED) is shown to decrease with increasing inflation pressure with a minimum of 0.0417 MPa at the highest inflation load, 827 kPa. In particular, the CED amplitudes over the entire duty cycle when the tire is inflated at 793 kPa is shown to be lower than those for the other inflation loads and does suggest a low rate of potential crack growth. The same explanation holds for the case where the truck travels empty (shown in Fig. 11b) with a slightly higher peak CED value at 827 kPa than at 793 kPa.

[Fig. 11a — Inflation pressure effect on CED: Loaded truck.][Fig. 11b — Inflation pressure effect on CED: Empty truck.]

Lake et al.¹⁸ reported that sufficient time is needed to maximize the benefits of SIC at a crack tip. In light of this, the effect of speed (frequency of loading the crack tip) on life was studied for the extreme internal pressures. Fig. 12a-b show fatigue life plots obtained each for tire travel velocities: 3.6 m/s and 12.07 m/s at inflation pressures 724 kPa and 827 kPa, respectively. The results show 27% and 70% more life for the respective internal pressures at 12.07 m/s than life estimates at speed case 3.6 m/s. This trend was least expected as higher speed meant insufficient loading time at the crack tip to allow significant SIC to occur. On the other hand, it could be said that the speeds involved are just not high enough to clearly show how strain rates influence the effects of SIC on fatigue life.

[Fig. 12ai — Effect of tire speed on fatigue life at 724 kPa internal pressure and 3.6 m/s speed.]

[Fig. 12aii — Effect of tire speed on fatigue life at 724 kPa internal pressure and 12.07 m/s speed.]

[Fig. 12bi — Effect of tire speed on fatigue life at 827 kPa internal pressure and 3.6

m/s speed.]

[Fig. 12bii — Effect of tire speed on fatigue life at 827 kPa internal pressure and 12.07 m/s speed.]

6. Conclusions

The fatigue behavior of tires is contingent on many factors. Three of the factors inflation pressure, machine weight, and travel speed—that relate to the mechanical load history class of factors have been discussed in this work. Fatigue and hyperplastic measurement data of the belt package compound were characterized for use in the finite element model of the 56/80R63 tire. The results obtained identifies the belt edges to be the most critical regions for crack nucleation.

The effect of strain-induced crystallization (SIC) on fatigue life has been shown to vary based on the loading conditions imposed on the tire. The results also corroborate reports in the literature that, in strain crystallizing rubber parts of a tire, increasing inflation loads prevents nonzero loading at a crack tip as the formation of crystallites in the process zone stops further crack growth. Among the inflation pressures studied, 793 kPa (115 psi) appeared to be the optimum one for the given operating conditions of the tire. Crack driving force on a potential cracking plane is shown to increase with an increase in axle load for a given internal pressure. The expected effect of speed on fatigue life in light of SIC could, however, not be determined directly and thus, forms a basis for further investigation in the

future.

References

- 1. Ebbott T. An application of finite element-based fracture mechanics analysis to cord-rubber structures. *Tire Science and Technology*. 1996; 24: 220-35.
- 2. Han Y, Becker EB, Fahrenthold EP and Kim D. Fatigue life prediction for cordrubber composite tires using a global-local finite element method. *Tire science and Technology*. 2004; 32: 23-40.
- 3. Ozelo R, Sollero P and Costa A. An alternative technique to evaluate crack propagation path in hyperelastic materials. *Tire Science and Technology*. 2012; 40: 42-58.
- 4. Wei Y-T, Tian Z-H and Du X. A finite element model for the rolling loss prediction and fracture analysis of radial tires. *Tire science and technology*. 1999; 27: 250-76.
- 5. Näser B, Kaliske M and Mars WV. Fatigue investigation of elastomeric structures. *Tire Science and Technology*. 2010; 38: 194-212.
- 6. Huang Y and Yeoh O. Crack initiation and propagation in model cord-rubber composites. *Rubber chemistry and technology*. 1989; 62: 709-31.
- 7. Li F, Liu J, Mars W, et al. Crack precursor size for natural rubber inferred from relaxing and non-relaxing fatigue experiments. *International Journal of Fatigue*. 2015; 80: 50-7.
- 8. Mars W. Multiaxial fatigue crack initiation in rubber. *Tire Science and Technology*. 2001; 29: 171-85.
- 9. CAT 795F AC Mining Truck Specifications.
- 10. Nyaaba W. *Thermomechanical Fatigue Life Investigation of an Ultralarge Mining Dump Truck Tire*. Missouri University of Science and Technology, 2017.
- 11. Ogden RW. Large deformation isotropic elasticity–on the correlation of theory and experiment for incompressible rubberlike solids. *Proc R Soc Lond A*. 1972; 326: 565-84.
- 12. Bhowmick AK. Threshold fracture of elastomers. *Polymer Reviews*. 1988; 28: 339-70.

- 13. Thomas A. Rupture of rubber. V. Cut growth in natural rubber vulcanizates. *Journal of Polymer Science Part A: Polymer Chemistry*. 1958; 31: 467-80.
- 14. Mars W and Fatemi A. A phenomenological model for the effect of R ratio on fatigue of strain crystallizing rubbers. *Rubber chemistry and technology*. 2003; 76: 1241-58.
- 15. Huneau B. Strain-induced crystallization of natural rubber: a review of X-ray diffraction investigations. *Rubber chemistry and technology*. 2011; 84: 425-52.
- 16. Kabe K and Koishi M. Tire cornering simulation using finite element analysis. *Journal of Applied Polymer Science*. 2000; 78: 1566-72.
- 17. Andonian AAT, Legge KC, Neubauer RA and Wells DE. Two piece tire with improved tire tread belt. Google Patents, 2007.
- 18. Lake G, Lawrence C and Thomas A. High-speed fracture of elastomers: Part I. *Rubber chemistry and technology*. 2000; 73: 801-17.